nuclear fusion
IAEA

PAPER • OPEN ACCESS

Negative triangularity scenarios: from TCV and AUG experiments to DTT predictions

To cite this article: A. Mariani *et al* 2024 *Nucl. Fusion* **64** 106024

OPEN ACCESS
IOP Publishing | International Atomic Energy Agency
Nuclear Fusion
Nucl. Fusion **64** (2024) 106024 (16pp)
https://doi.org/10.1088/1741-4326/ad6ea0

Negative triangularity scenarios: from TCV and AUG experiments to DTT predictions

A. Mariani[1,*], L. Aucone[2], A. Balestri[3], P. Mantica[1], G. Merlo[4], R. Ambrosino[5], F. Bagnato[3], L. Balbinot[6], J. Ball[3], T. Bolzonella[7], D. Brioschi[2], I. Casiraghi[1], A. Castaldo[8], S. Coda[3], L. Frassinetti[9], V. Fusco[8], T. Happel[10], J. Hobirk[10], P. Innocente[7], R.M. McDermott[10], P. Muscente[7], T. Pütterich[10], O. Sauter[3], F. Sciortino[10], M. Vallar[3], B. Vanovac[11], N. Vianello[11], G. Vlad[8], C.F.B. Zimmermann[10], the EUROfusion Tokamak Exploitation team[a], the TCV Team[b] and the ASDEX Upgrade Team[c]

[1] Institute for Plasma Science and Technology, CNR, Milano, Italy
[2] Department of Physics 'G. Occhialini', University of Milano-Bicocca, Milano, Italy
[3] École Polytechnique Fédérale de Lausanne (EPFL), Swiss Plasma Center (SPC), Lausanne, Switzerland
[4] Oden Institute for Computational Engineering and Sciences, University of Texas at Austin, Austin, TX, United States of America
[5] Università degli Studi di Napoli Federico II Napoli, Italy
[6] Università della Tuscia, Dipartimento di Economia, Ingegneria, Societá e Impresa (DEIM), Viterbo, Italy
[7] Consorzio RFX (CNR, ENEA, INFN, Università di Padova, Acciaierie Venete SpA), Padova, Italy
[8] ENEA C.R.Frascati, Frascati, Italy
[9] Fusion Plasma Physics, ECSS, KTH Royal Institute of Technology Stockholm, Sweden
[10] Max-Planck-Institut für Plasmaphysik, Garching, Germany
[11] Plasma Science and Fusion Center, Massachusetts Institute of Technology, Cambridge, MA, United States of America

E-mail: alberto.mariani@istp.cnr.it

Received 8 March 2024, revised 28 June 2024
Accepted for publication 13 August 2024
Published 27 August 2024

Abstract

Experiments, gyrokinetic simulations and transport predictions were performed to investigate if a negative triangularity (NT) L-mode option for the Divertor Tokamak Test (DTT) full-power scenario would perform similarly to the positive triangularity (PT) H-mode reference scenario, avoiding the harmful edge localized modes (ELMs). The simulations show that a beneficial effect of NT coming from the edge/scrape-off layer (SOL) region $\rho_{\mathrm{tor}} > 0.9$ is needed to allow the actual NT L-mode option to perform like the PT H-mode. Dedicated experiments at TCV and AUG, with DTT-like shapes, show an optimistic picture. In TCV, experiments indicate that even with the relatively small triangularity of the DTT NT scenario, a large beneficial effect of NT comes from the plasma edge and SOL, allowing NT L-modes to outperform PT L-modes with the same

[a] See Joffrin *et al* 2024 (https://doi.org/10.1088/1741-4326/ad2be4) for the EUROfusion Tokamak Exploitation Team.
[b] See Reimerdes *et al* 2022 (https://doi.org/10.1088/1741-4326/ac369b) for the TCV Team.
[c] See Zohm *et al* 2024 (https://doi.org/10.1088/1741-4326/ad249d) for the ASDEX Upgrade Team.
[*] Author to whom any correspondence should be addressed.

power input, reaching the same central pressures as PT H-modes with twice as much applied heating power. For AUG, NT plasmas go into H-mode more easily than for TCV, but always present much smaller pedestals compared with PT plasmas with the same input power, showing a much weaker or absent ELM activity. However, NT has a smaller beneficial effect for AUG than for TCV, with NT pulses outperforming PT pulses with the same input power only for an ECRH-only case with relatively low input power. For the considered AUG cases, PT pulses perform better than NT ones at higher ECRH power or with mixed NBI and ECRH power. Based on this analysis, the NT option is a viable alternative for the DTT full power scenario, providing high performance plasmas with reduced or absent ELMs.

Keywords: negative triangularity, heat transport, turbulence, gyrokinetics, DTT, TCV, AUG

(Some figures may appear in colour only in the online journal)

1. Introduction

Experiments performed at TCV [1–3], DIII-D [4–6] and AUG [7] indicate it is possible, in some cases, for negative triangularity (NT) plasmas [8], i.e. plasmas with D-shape convexity directed towards the inside of the torus instead of the outside, to perform comparably to H-mode plasmas with standard 'D-shaped' cross-section (positive triangularity: PT). In NT plasmas, an H-mode-like plasma performance can be achieved with reduced or even absent edge localized modes (ELMs), detrimental instabilities which could potentially damage the tokamak in fusion reactor regimes [9, 10]. Since the physics behind the performance improvement in NT compared to PT is not yet fully understood, current experimental, theoretical, and numerical analysis is ongoing in order to investigate it [11]. This is required for extrapolating to possible future NT fusion reactors [12, 13]. An NT option is under design for the full-power scenario [14] of the Divertor Tokamak Test (DTT) facility [15]. DTT is under construction in Italy and aims to test alternative designs and materials for the divertor, within the roadmap to the EU DEMO [16]. Since DTT is still under construction, it is impossible to perform direct experiments to test such scenarios. Therefore, two different approaches were followed by the authors to investigate the predicted performance of the DTT NT scenario: first, a numerical modeling effort by means of predictive transport simulations and gyrokinetic simulations was performed [17, 18], then dedicated experiments at TCV [19] and AUG [20] were carried out, obtaining plasmas with NT shape close to the DTT one at reduced volume. The outcomes of these analyses are collected here, comparing the results that were obtained with the numerical and experimental approaches, in order to construct a coherent picture of the underlying physics.

The numerical analysis of the DTT scenario was carried out as follows: predictive simulations with the transport code ASTRA [21, 22], coupled with the quasilinear model TGLF [23] with the saturation rule SAT2, were run first. The PT H-mode reference DTT full-power scenario with neon seeding was compared with the NT L-mode option, calculating, self-consistently, the NBI/ECRH/ICRH power input and the impurity profiles. Then, these results were validated at two selected radii by gyrokinetic simulations with the GENE code [24, 25].

In TCV experiments, in addition to the PT H-mode/NT L-mode comparisons, PT L-modes were obtained to understand how the transport in L-mode improves when changing the sign of the triangularity from PT to NT. Moreover, different heating mixes were applied, namely NBI-only, mixed NBI/ECRH and ECRH-only, to carry out a thorough analysis. When NBI injection was present, PT/NT L-modes with lower NBI power were compared with PT H-modes with double NBI power. The results were then interpreted with ASTRA-TGLF SAT2 transport simulations, and GENE at selected radii.

Unlike TCV plasmas, NT discharges in AUG tend to go into H-mode when operated with the ion ∇B drift pointing towards the X-point (called 'favorable configuration'), compared with the opposite configuration where the ion ∇B drift points in the opposite direction to the X-point (called 'unfavorable configuration'). Thus, both 'favorable' and 'unfavorable' configurations were obtained, to include in the PT/NT comparisons at least one NT discharge operating in L-mode. PT discharges from the AUG database, with high shaping and comparable q (same current and field), were compared with the NT pulses. The experiments were interpreted with ASTRA-TGLF SAT2 simulations.

2. DTT/TCV/AUG predictive transport modeling and TCV/AUG experimental results

The DTT full-power scenario is being designed by means of integrated modeling [14, 26]. The reference PT is an H-mode with $B_t = 5.85\,\mathrm{T}/I_p = 5.5\,\mathrm{MA}$ and neon seeding, where 45 MW are injected with an ECRH+NBI+ICRH heating mix ($P_{ECRH} = 32\,\mathrm{MW}$, $P_{ICRH} = 8\,\mathrm{MW}$, $P_{NBI} = 10\,\mathrm{MW}$). The total ECRH, NBI, and ICRH input power is kept fixed for the NT scenario, while the power deposition profiles are computed self-consistently in the two PT/NT options. B_t is also kept fixed, while a lower $I_p = 4\,\mathrm{MA}$ plasma current is considered for the NT scenario, since a plasma current limit of 4 MA for the Single Null NT configuration is present, due to the engineering constraints on the maximum forces on the poloidal field

system. This also allows us to have similar q_{95} for the PT and NT options, since the different PT/NT shapes compensate for the I_p difference. Finally, the NT case was assumed to be an L-mode, and the possible beneficial effects of reversing the triangularity of the DTT PT scenario, coming from the plasma edge and/or from the scrape-off layer (SOL), were neglected [18]. As a consequence, the predicted performance for the NT scenario is a lower boundary, which could be improved by accounting for a beneficial effect of reversing the triangularity coming from the edge-SOL. We refer to [18] for more information about how the PT H-mode pedestal and NT L-mode edge n, T boundary conditions were set for the DTT scenarios.

The effect of changing the triangularity of the DTT full-power scenario from positive to negative on the plasma performance was investigated by our group by running numerical simulations, and by carrying out experiments with similar shapes at TCV and AUG. The plasma shapes of the PT/NT DTT full-power scenarios, as well as the main geometrical parameters of interest for the analysis, such as the safety factor q, the triangularity δ and the elongation κ, defined as in [36], are shown in figure 1 in black. As can be observed in figure 1(a), the DTT PT scenario presents an almost up-down symmetric shape, while the NT shape is up-down asymmetric.

Here, $\rho_{\rm tor} = \sqrt{\Phi/\Phi_{\rm edge}}$ is the normalized toroidal radius, where Φ is the flux of the toroidal magnetic field. A selection of corresponding quantities from TCV and AUG experiments are shown in red and blue, respectively. As can be observed in figures 1(a)/(c), the DTT shapes and triangularities were reproduced with a good approximation in TCV and AUG experiments. To avoid Vertical Displacement Events (VDEs), the elongation was reduced in TCV and AUG pulses with respect to the DTT reference profiles (figure 1(d)). For DTT, the LCFS shapes were computed with the free boundary CREATE-NL solver [27] and the equilibria inside the last close flux surface (LCFS) with ASTRA using the SPIDER equilibrium code [28]. The TCV experimental equilibria are obtained with LIUQE [29], while the AUG equilibria with IDE [30].

2.1. Predicted (DTT) and experimental (TCV/AUG) profiles

Let us now consider the numerical and experimental results. The predictive transport simulation output is shown for DTT, where the experiments are not yet possible, while the experimental results are reported for TCV and AUG. The kinetic profiles of pressure, density and temperature are shown in figures 2 and 3.

The results of the ASTRA-TGLF predictive transport simulations of the DTT PT H-mode and NT L-mode scenarios, performed with density and temperature boundary conditions at $\rho_{\rm tor} = 0.94$, are shown in red and blue, respectively, in figure 2(a). They show that the NT L-mode scenario is not able to recover the loss of the PT H-mode pedestal and achieve similar total pressures $p_{\rm tot} \simeq n_e T_e + n_i T_i + n_{\rm Ne} T_i$. This being possibly due to the $|\delta|$ value not sufficiently large to result in a significant improvement of the core transport. More details

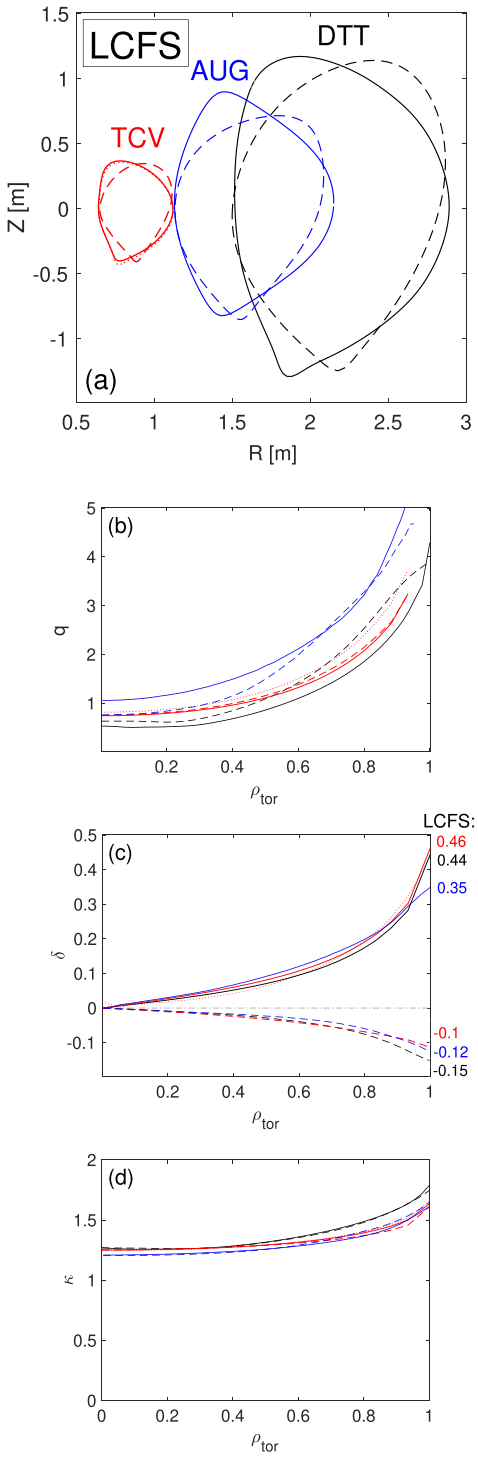

Figure 1. (a) Plasma shapes (last close flux surface: LCFS) for DTT PT/NT scenarios (black solid/dashed), TCV pulses #73391/#73388/#73382 (PT H-mode/PT L-mode/NT L-mode, red solid/dotted/dashed) and AUG pulses #36157/#40473 (PT/NT H-modes, blue solid/dashed). Radial profiles of (b) safety factor q, (c) triangularity δ and (d) elongation κ, corresponding to the cases in (a), following the same color/line style codes.

on the DTT predicted n_e, T_e and T_i profiles are given in the first column of figure 3, following the same color code. The T_e predictions inside $\rho_{\rm tor} = 0.2$ should not be trusted, since

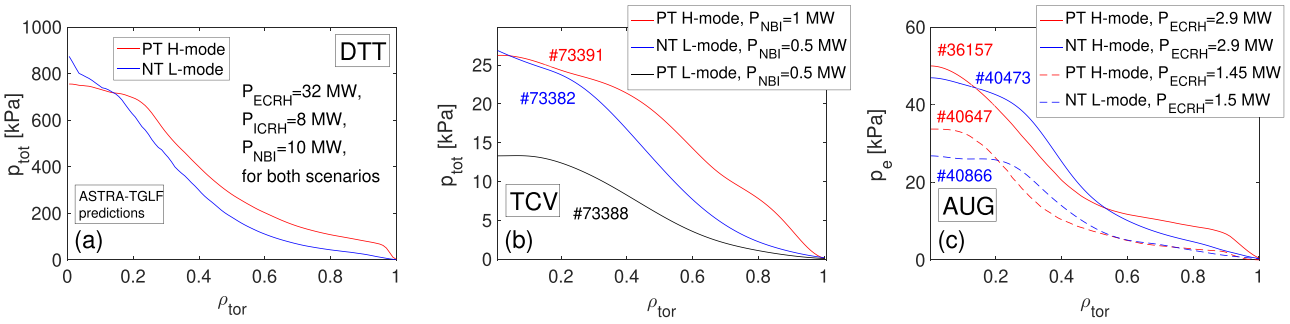

Figure 2. (*a*) DTT ASTRA-TGLF predicted p_{tot} profiles: PT reference H-mode full-power scenario with neon seeding and corresponding NT L-mode scenario, both with injected $P_{ECRH} = 32$ MW, $P_{ICRH} = 8$ MW, $P_{NBI} = 10$ MW. Reproduced from [18]. © 2024 The Author(s). Published by IOP Publishing Ltd on behalf of the IAEA. All rights reserved CC BY 4.0. (*b*) TCV experimental p_{tot} profiles: comparison of higher NBI power PT H-mode (#73391, $t = 0.72$–0.74 s, $P_{NBI} = 1$ MW) with half power PT/NT L-modes (#73388/#73382, both for $t = 0.68$–0.79 s). Reproduced from [19]. © The Author(s). Published by IOP Publishing Ltd. CC BY 4.0. (*c*) AUG experimental p_e profiles: PT/NT H-modes with $P_{ECRH} = 2.9$ MW (#36157, $t = 4.6$–4.9 s/#40473, $t = 3$–3.5 s), PT/NT H/L-modes (#40647, $t = 3.4$–4 s/#40866, $t = 2.6$–2.8 s). Reproduced from [20]. © The Author(s). Published by IOP Publishing Ltd. CC BY 4.0.

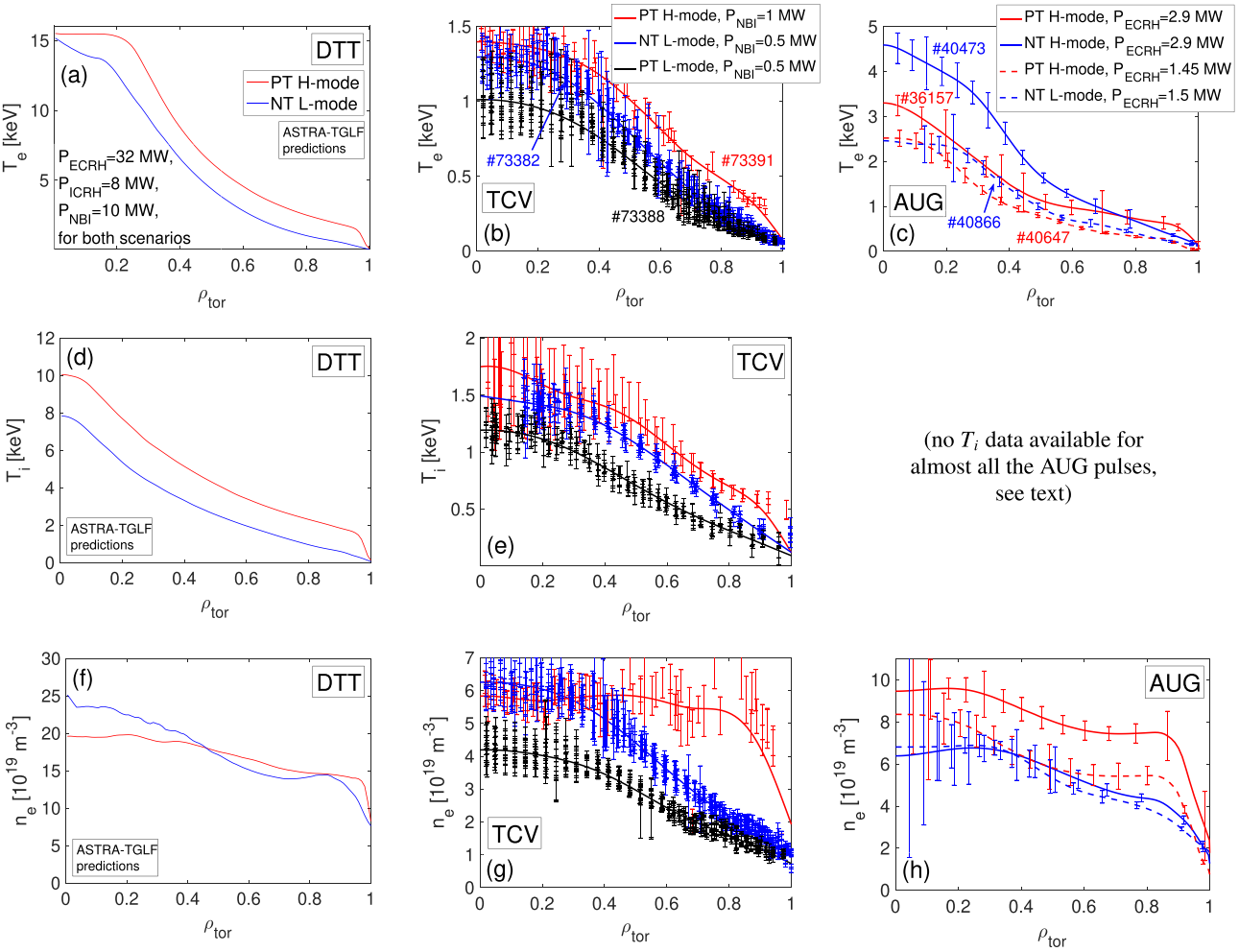

Figure 3. T_e (first row), T_i (second row) and n_e (third column) profiles, with columns corresponding to the cases of figure 2. DTT (first column): ASTRA-TGLF predicted profiles; TCV (second column): experimental profiles; AUG (third column): experimental profiles. (*a*), (*d*), (*f*) Reproduced from [18]. © 2024 The Author(s). Published by IOP Publishing Ltd on behalf of the IAEA. All rights reserved CC BY 4.0. (*b*), (*e*), (*g*) Reproduced from [19]. © The Author(s). Published by IOP Publishing Ltd. CC BY 4.0, while (*c*), (*h*) Reproduced from [20]. © The Author(s). Published by IOP Publishing Ltd. CC BY 4.0.

TGLF predicts unrealistically high electron heat transport in that region [18]. One can observe that, even though the NT electron density recovers and exceeds the PT central values, both T_e and T_i for NT stay well below the PT counterparts across the full plasma radius, preventing the total pressure from recovering the loss of the PT H-mode pedestal for the most of the radial domain, resulting in poorer performance for NT. We point out that TGLF uses an up-down symmetric Miller local analytic equilibrium, only accounting for elongation κ and triangularity δ:

$$R(\theta) - R_0 = a\cos\left[\theta - \sin^{-1}(\delta)\sin(\theta)\right] \quad (1)$$

$$Z(\theta) - Z_0 = a\kappa\sin(\theta)\,, \quad (2)$$

where R_0, Z_0, a (geometrical minor radius) are defined as in [36], and the triangularity δ is obtained as an average of the upper and lower triangularities. As a consequence, TGLF misses more than half of the upper NT absolute value for the DTT NT scenario, in addition to missing all the up-down asymmetry of the DTT NT 'teardrop' geometry. As a consequence, ASTRA-TGLF could underpredict the beneficial effect of the NT. Present interfaces to TGLF in the main available transport codes are limited to Miller geometry, although work is ongoing to expand the interface to general geometry. However, one could expect that when increasing the absolute value of the negative δ, the NT scenario could perform better. Therefore, a new version of the NT scenario is under design, with larger negative upper triangularity and reduced volume, to satisfy the engineering constraints. In addition, the possibility for the DTT NT scenario to access larger edge pressure gradients than L-mode-like is open, still not reaching values compatible with H-mode pedestals due to the inhibited access to the second stability region of high-n ballooning modes for sufficiently negative δ [31–35]. This could contribute to the possible improvement of the DTT NT scenario performance.

On the contrary, TCV experiments draw a much more optimistic picture. For clarity, figures 2 and 3 show the same cases for both TCV and AUG. For TCV, the cases with only NBI are shown: a larger NBI power PT H-mode (red) is compared with half power PT(black)/NT(blue) L-modes. Figure 2(*b*) shows that NT L-mode performs significantly better than PT L-mode, reaching a central total pressure $p_{tot} \simeq n_e T_r + n_i T_i + n_C T_i$ (C indicates the main impurity: carbon) comparable to PT H-mode, which has double injected NBI power. This large beneficial effect of NT is shared by all the main kinetic profiles, i.e. T_e, T_i and n_e, as can be observed in the second column of figure 3. Differently from what was predicted by the DTT simulations of [18], this is exactly how one would wish NT to behave. A similar optimistic picture has also been obtained for mixed ECRH/NBI pulses and ECRH-only ones (for ECRH-only pulses only a PT/NT L-mode couple was obtained) [19]. The NBI heated cases present the largest beneficial effect.

Considering AUG, the picture is more complicated. Let us start from the comparison of a PT and a NT ELMy H-mode with ECRH-only (same ECRH power). This is shown in figure 2(*c*) and in the third column of figure 3 with red/blue solid lines. The ion temperature has not been shown for consistency, since it was only measured for pulse #40473 at the considered time slice. Consistently, only the electron pressure p_e is shown. The data show that the NT discharge presents a smaller pedestal, but overall, the PT/NT p_e profiles are roughly similar, with the NT profile recovering the PT one outside mid-radius. Looking at the single n, T profiles, the NT pulse recovers the PT T_e values for $\rho_{tor} > 0.8$, reaching 40% larger central values. However, this is only partially due to a reduced heat transport in NT. Indeed, part of this improvement comes from the 30% smaller central density for NT compared with PT, with same heating, resulting in a larger T_e. The smaller density of the NT pulse, however, reduces the electron-ion collisional energy exchange and, given that these cases are electron heated, should lead to a smaller T_i. This is indeed what is found by predicting T_i with ASTRA-TGLF, as will be shown in the following. As a consequence, even though the p_e are similar for PT/NT, p_i is smaller for NT. T_i was only measured for the NT H-mode pulse #40473 (see figure 9(*e*) in the following), and presents central $T_i/T_e \sim 40\%$, consistent with the ECRH heating. Now, let us consider an H-mode/L-mode PT/NT couple that was obtained creating the L-mode in the 'unfavourable configuration'. The results are shown by dashed lines. Here, the NT L-mode recovers the central T_e of the PT H-mode, with a slightly smaller central density, thus obtaining a similar electron pressure. For this case, as will be shown in detail in the following, ASTRA-TGLF predicts larger T_i for the NT case, resulting in a larger p_i. However, in this case the PT plasma is an ELM-free H-mode (EDA) [37, 38], therefore, there is no practical gain for this case when changing the triangularity to NT, since in both pulses there are no ELMs. Finally, NT H-modes with ECRH+NBI were obtained at AUG. The results are not shown here for brevity, and we refer to [20] for more details. The NT pulses were compared with PT H-modes with the same heating power. A couple of discharges with PT/NT DTT-like shapes were obtained, but the PT H-mode has a much larger density, leading to lower p_i for the NT plasma. A couple of PT/NT pulses with ECRH+NBI were obtained, matching both the heating power and the density, but for this couple the PT geometry is different from the DTT PT scenario, with reduced triangularity ($\delta_{LCFS} = 0.26$). For this case, the NT plasma performs better than the PT one, but probably due to the reduced positive δ of the PT counterpart. As a final remark, the pedestal height, and therefore the intensity of the ELM activity, is much reduced in NT pulses, compared with the corresponding PT ones [39]. Summing up, in AUG, even though it is possible to weaken the ELMs by changing the triangularity to negative, it is not always possible to reach a similar or larger performance. In particular, it is only possible to reach higher central ion pressure for NT for the lower power ECH only case and for a mixed NBI/ECRH case with reduced PT. Therefore, the beneficial effect of NT seems to be larger for TCV than for AUG. The reason for this difference is still to be understood. A possible evident difference could be the wall material, which is carbon for TCV and tungsten for AUG and DTT. A detailed analysis of the effect of impurities on the heat transport in the plasma edge of TCV and AUG is then planned

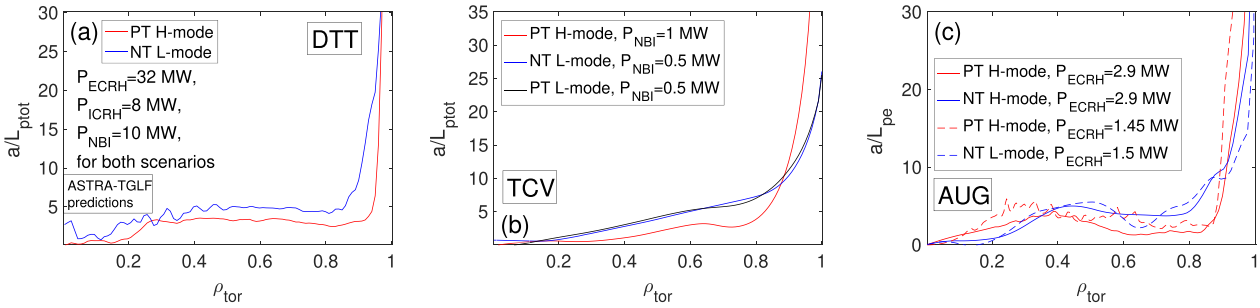

Figure 4. Normalized logarithmic gradients of $p_{\rm tot}$, corresponding to the profiles of figure 2, for DTT (a), TCV (b) and AUG (c). (a) Reproduced from [18]. © 2024 The Author(s). Published by IOP Publishing Ltd on behalf of the IAEA. All rights reserved CC BY 4.0.

as a future work. In addition, finite-size effects (global effects) could potentially affect the relative transport levels for PT/NT plasmas for the relatively small TCV plasmas [40, 41], but they are expected to be small for DTT and AUG, which are relatively larger machines. To investigate this second possibility, global GENE runs of TCV NBI-only PT/NT pulses are ongoing. However, the global effects are not likely to be a good candidate, since the TCV PT-NT L-modes at $\rho_{\rm tor} = 0.95$ display rather small $\rho^\star = \rho_{\rm s}/a \sim 1/357 - 1/278$ values. In addition, flux-tube gyrokinetic simulations are already able to explain and even overpredict the direct beneficial effect of NT on TCV plasmas, as will be shown in the following.

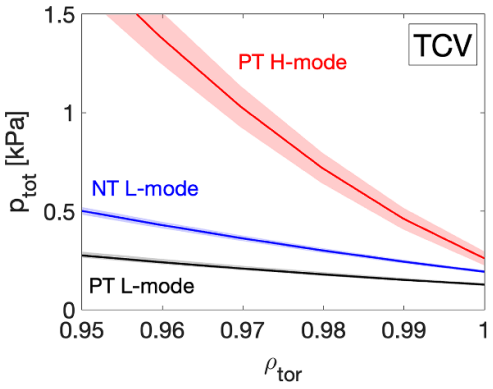

Figure 5. Total pressure profiles of TCV NBI-only pulses in the plasma edge (detail of figure 2 (b)). Reproduced from [19]. © The Author(s). Published by IOP Publishing Ltd. CC BY 4.0.

2.2. *Turbulence drive: logarithmic gradient of n, T*

To investigate the role that the transport inside the separatrix has on the beneficial effect of the NT on the kinetic profiles, one can first look at the normalized logarithmic gradients $a/L_{\rm ptot} = -{\rm d}({\rm log}\, p_{\rm tot})/{\rm d}\rho_{\rm tor}$ of the total pressure ($a/L_{\rm pe}$ for AUG, where the $T_{\rm i}$ measurements are missing). In the definition of the normalized logarithmic gradients, $a = \sqrt{\Phi_{\rm edge}/\pi B_0}$ provides an estimate of the average minor radius of the tokamak. The results are shown in figures 4(a)–(c), for DTT/TCV/AUG, respectively, corresponding to the pressure profiles of figures 2(a)–(c). One notes that, when comparing PT H-modes with NT L-modes, $a/L_{\rm p}$ is always larger for the H-mode outside the pedestal top, as can be seen by comparing with figure 2, while it is smaller inside it, due to the common flattening of the kinetic profiles inside the pedestal of an H-mode, due to transport physics. The same holds for the corresponding $T_{\rm e}$, $T_{\rm i}$, and $n_{\rm e}$ profiles, shown in figure 6. This can be seen in both DTT and AUG cases. For the AUG higher power PT/NT H-mode/H-mode comparison, one sees that the NT logarithmic gradients are larger for $\rho_{\rm tor} < 0.9$, similarly to the lower ECRH power PT/NT H-mode/L-mode comparison.

The TCV results can help better understand where the effect of the triangularity impacts the L-mode profiles, since both PT and NT L-modes are available and have the same injected NBI power. Indeed, when looking at figure 4(b), one observes an interesting feature: the PT/NT L-modes have almost equal normalized logarithmic gradient of the total pressure $a/L_{\rm ptot}$ along the whole radius. Therefore, the effect of NT on the total pressure, which results in an almost double central value for the NT L-mode, is just due to the fact that the NT pulse has almost double the total pressure at the separatrix (see figure 5). Indeed, if two radial profiles have the same logarithmic gradient, their ratio is a constant. When considering the logarithmic gradients of the single $T_{\rm e}$, $T_{\rm i}$, and $n_{\rm e}$ profiles (second column of figure 6), one sees that a strong beneficial effect of NT is present for $T_{\rm e}$ for $\rho_{\rm tor} > 0.9$, and in the same radial region a milder beneficial effect is also found for $T_{\rm i}$, and $n_{\rm e}$. NT is also found to increase the logarithmic gradients of the kinetic profiles for the ECRH and NBI/ECRH cases, outside $\rho_{\rm tor} = 0.8$ [19]. For the NBI-only case, this beneficial effect on a/L_{Te}, a/L_{Ti}, and a/L_{ne} could seem in contrast with the fact that $a/L_{\rm ptot}$ is the same for PT and NT pulses. The reason for this apparent disagreement is that for this particular pair of pulses, carbon impurity accumulates at the edge, with larger accumulation for the PT case ($n_{\rm c}/n_{\rm e}$(PT, $\rho_{\rm tor} = 1) \sim 13\%$, $n_{\rm c}/n_{\rm e}$(NT, $\rho_{\rm tor} = 1) \sim 6\%$) leading, based on neutrality $n_{\rm i} = n_{\rm e} - 6n_{\rm c}$, to a larger a/L_{ni} for PT compared to NT. This compensates the gain in a/L_{Te}, a/L_{Ti}, and a/L_{ne}, giving the same $a/L_{\rm ptot}$ for PT and NT L-modes. Therefore, for this case only, the improvement of a/L_{Te}, a/L_{Ti}, and a/L_{ne} inside the separatrix is essential to compensate the smaller $n_{\rm i}$ peaking due to carbon accumulation. For the ECRH and NBI/ECRH cases, $a/L_{\rm ptot}$ is larger for NT L-modes compared with PT L-modes outside $\rho_{\rm tor} = 0.8$ [19].

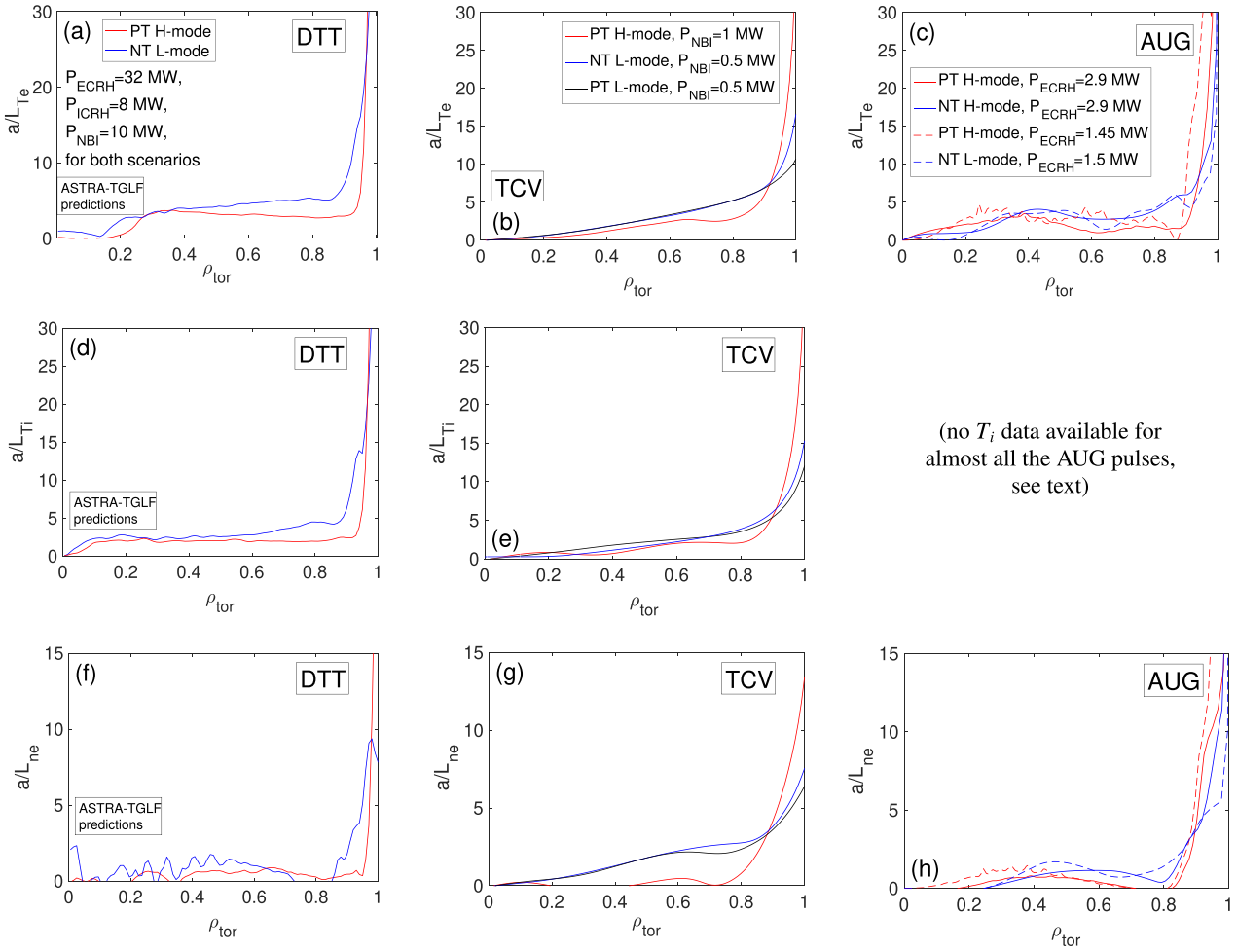

Figure 6. Normalized logarithmic gradients of T_e (first row), T_i (second row) and n_e (third row), corresponding to the profiles of figure 3, for DTT (first column), TCV (second column) and AUG (third column). (*a*), (*d*), (*f*) Reproduced from [18]. © 2024 The Author(s). Published by IOP Publishing Ltd on behalf of the IAEA. All rights reserved CC BY 4.0. (*b*), (*e*), (*g*) Reproduced from [19]. © The Author(s). Published by IOP Publishing Ltd. CC BY 4.0, while (*c*), (*h*) Reproduced from [20]. © The Author(s). Published by IOP Publishing Ltd. CC BY 4.0.

These results suggest that, for the considered cases with DTT-like shapes, when comparing PT/NT L-modes, a beneficial effect of NT comes from reduced transport in the edge region $\rho_{tor} > 0.8$ while, when comparing PT/NT H-modes, the beneficial effect starts more inside.

The analysis of the logarithmic gradient of p_{tot} for the TCV NBI-only cases suggested that the boundary conditions of the kinetic profiles at the separatrix could be the main contributors to the better properties of NT compared with PT pulses. To test the effect of the n, T boundary conditions at the LCFS, a numerical exercise was performed for the TCV NBI-only cases by considering the T_e, T_i, and n_e profiles. The impact of changing n, T at $\rho_{tor} = 1$ on the corresponding central values was roughly evaluated by integrating the n, T profiles of the PT L-mode for $\rho_{tor} < 1$, keeping fixed the PT L-mode logarithmic gradients but imposing the n, T values at $\rho_{tor} = 1$ from the corresponding NT L-mode (and vice-versa). It is found that the difference of n, T at the LCFS contributes roughly half of the difference between the central values between PT and NT L-modes, as is shown for T_e in figure 7(*a*) (for T_i, this is only true outside $\rho_{tor} \sim 0.6$, since inside that radius the transport properties become worse for NT, but the triangularity should not matter for $\rho_{tor} < 0.6$). The additional half comes from the improved logarithmic gradients in NT. This suggests that the physics of the SOL can play an important role, contributing a large portion of the beneficial effect of NT.

This is confirmed for TCV, where steeper n, T profiles are found for NT L-modes than for PT L-modes in the SOL (corresponding to a narrower λ_q, in agreement with what was reported in [42, 43]). The T_e profiles of the TCV NBI-only cases in the edge-SOL are shown in figure 8(*a*). For AUG, even though the experimental measurements do not allow us to estimate with precision if the n, T profiles are different for PT and NT pulses, the NT cases do not present a typical H-mode pedestal, while this is compensated by larger gradients at the LCFS. The T_e profiles of the AUG ECRH-only cases in the

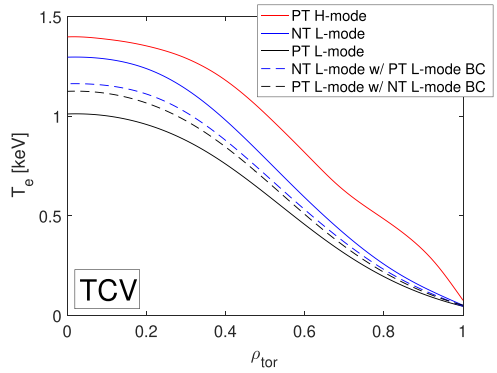

Figure 7. Electron temperature profiles of the NT L-mode (blue), PT L-mode (black) and PT H-mode (red) scenarios of the TCV NBI-only case. The solid lines correspond to the experimental kinetic profiles, the dashed lines indicate scenarios where we artificially reconstructed a profile by keeping fixed the logarithmic gradients and swapping boundary conditions (BC) between NT and PT. Reproduced from [19]. © The Author(s). Published by IOP Publishing Ltd. CC BY 4.0.

edge-SOL are shown in figure 8(*b*). Unfortunately, for AUG PT L-modes were not obtained to compare with. The overall picture agrees with what is emerging within the working group of the EUROfusion TSVV task 2, where NT L-modes are found to produce an intermediate 'proto-pedestal' between the PT H-mode pedestal and the L-mode edge, probably due to a reduced turbulent transport around the separatrix.

Summing up, based on the analysis of TCV and AUG experiments with DTT-like shapes, given the relatively small $|\delta|$ of the NT scenario, a large part of the beneficial effect of NT could come from the far edge $\rho_{\rm tor} > 0.9$, or even from the SOL, through the boundary conditions of n, T at the LCFS. Therefore, in order to estimate how these contributions could modify the results of the DTT PT/NT comparison, a rough estimate of the possible effect of the edge-SOL was done, assuming that it could be similar for the DTT NT scenario and for the TCV experiments. In figure 8(*c*), the modification of the DTT NT $T_{\rm e}$ profile that is predicted by the ASTRA-TGLF simulations with boundary conditions at $\rho_{\rm tor} = 0.94$, due to a possible beneficial effect of NT coming from $\rho_{\rm tor} > 0.94$, is shown. The resulting increase of $T_{\rm e}$ is of $+30\%$. The 'improved' electron temperature profiles (black lines) are computed as

$$\bar{T}_{\rm e}\left(\rho_{\rm tor}\right) = \bar{T}_{\rm e}\left(\bar{\rho}_{\rm tor}\right) e^{\int_{\bar{\rho}_{\rm tor}}^{\rho_{\rm tor}} \frac{a}{L_{T_{\rm e}}}\, d\rho'_{\rm tor}}\,, \tag{3}$$

with $\bar{\rho}_{\rm tor} = 0.94, 1$ and $\bar{T}_e(\bar{\rho}_{\rm tor}) = T_e(\bar{\rho}_{\rm tor}) * 1.3, T_e(\bar{\rho}_{\rm tor}) * 1.15$, respectively, corresponding to the solid and dashed lines, where $a/L_{T{\rm e}}$ is kept equal to the ASTRA-TGLF output for the DTT NT scenario. The solid black NT L-mode profile is now able to reach the same central temperature as the PT H-mode. In this hypothetical case, the beneficial effect of NT is equally split between a $+15\%$ increase of $T_{\rm e}$ at the LCFS, coming from an improved heat transport for NT in the SOL, and an additional $+15\%$ coming from a possibly weaker heat transport for $\delta < 0$ in the $0.94 < \rho_{\rm tor} < 1$ region. These values are

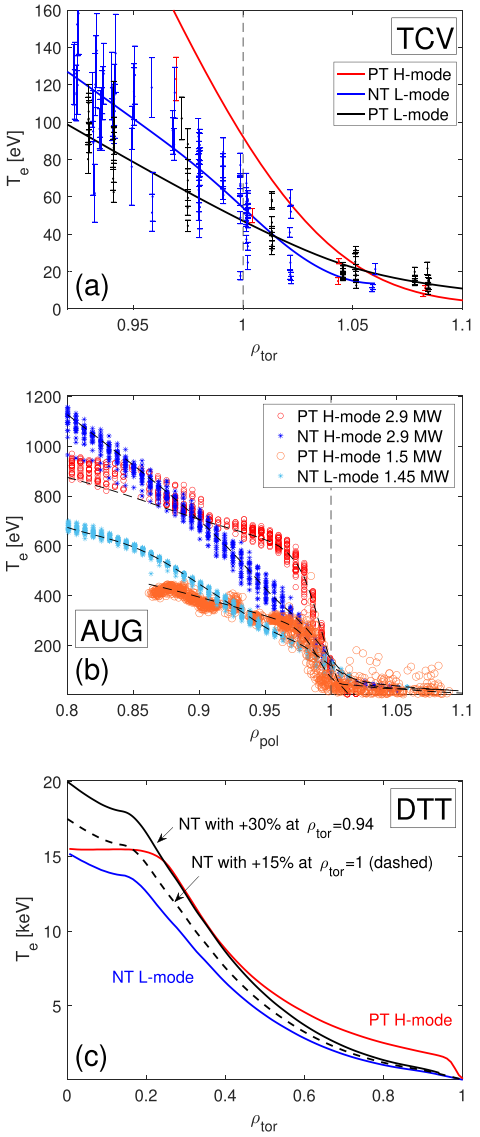

Figure 8. (*a*) and (*b*) $T_{\rm e}$ experimental profiles in the plasma edge and SOL, for TCV NBI-only cases and AUG ECRH-only cases, respectively. (*c*) Possible beneficial effect of reversing the sign of the triangularity on the $T_{\rm e}$ profile of the DTT NT scenario, coming from $\rho_{\rm tor} > 0.94$. The dashed black curve is obtained by increasing by $+15\%$ the $T_{\rm e}$ value at the LCFS and keeping fixed $a/L_{T{\rm e}}$ inside $\rho_{\rm tor} = 1$ while, for the solid black curve, $T_{\rm e}$ is increased by $+30\%$ at $\rho_{\rm tor} = 0.94$ and then, similarly to the dashed one, $a/L_{T{\rm e}}$ is kept fixed inside that radius. (*a*) Reproduced from [19]. © The Author(s). Published by IOP Publishing Ltd. CC BY 4.0. (*c*) Reproduced from [18]. © 2024 The Author(s). Published by IOP Publishing Ltd on behalf of the IAEA. All rights reserved CC BY 4.0.

roughly compatible with the effect that is observed in TCV NBI-only cases when comparing PT/NT L-modes with the same input power.

2.3. Comparison: experimental/predicted TCV/AUG profiles

ASTRA-TGLF (SAT2) predictive simulations were also run for the TCV and AUG experiments. The results for the TCV cases with NBI-only and AUG cases with ECRH-only are

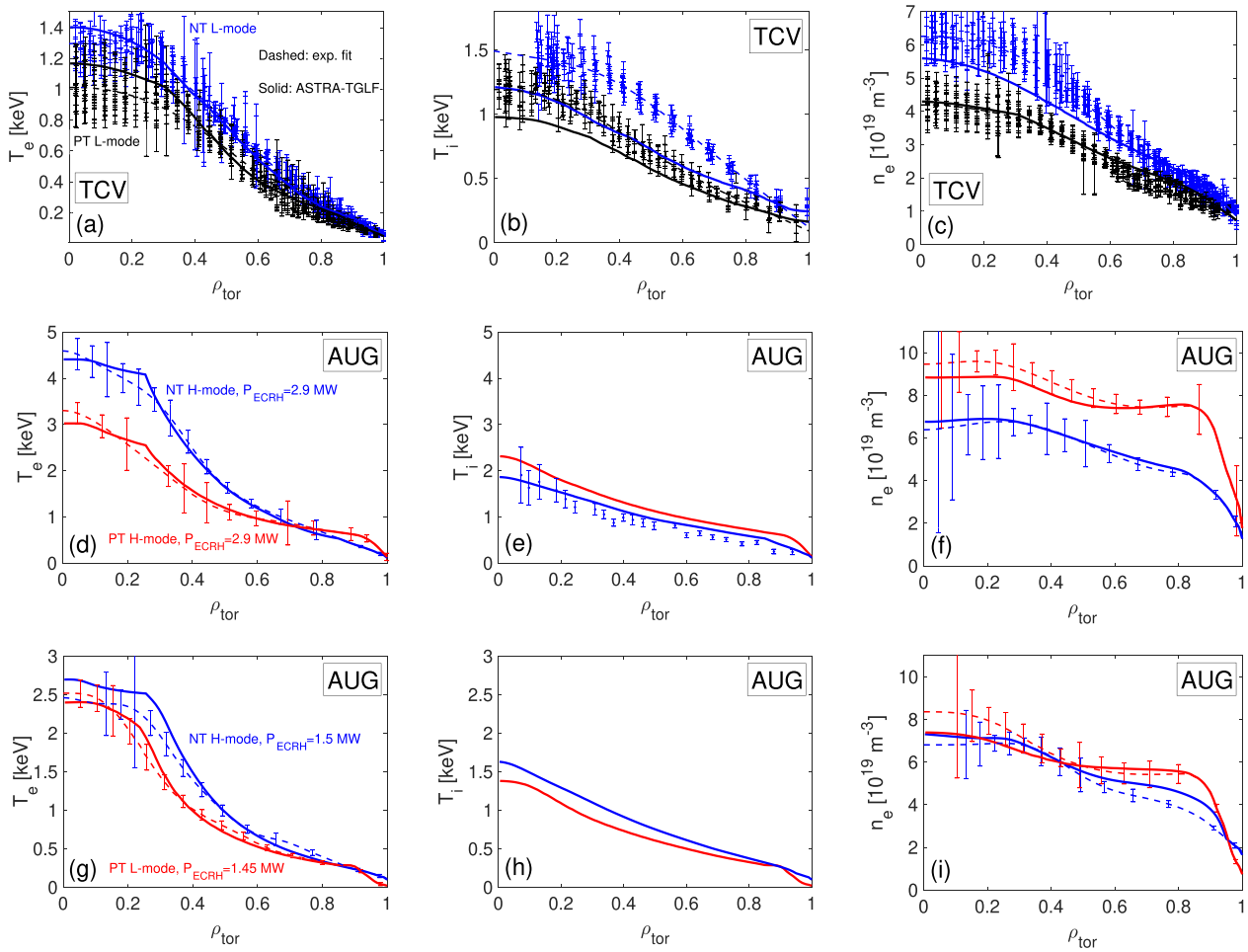

Figure 9. ASTRA-TGLF predictive transport simulations. The predicted $T_e/T_i/n_e$ profiles (solid thick lines) are shown in the first/second/third column, respectively, and compared with the experimental data, when available. The dashed lines indicate the fit of the experimental data. (*a*)–(*c*) TCV NBI-only L-modes; (*d*)–(*f*) AUG ECRH-only higher power H-modes; (*g*)–(*i*) AUG ECRH-only lower power PT/NT H-mode/L-mode couple. (*a*)–(*c*) Reproduced from [19]. © The Author(s). Published by IOP Publishing Ltd. CC BY 4.0. (*d*)–(*i*) Reproduced from [20]. © The Author(s). Published by IOP Publishing Ltd. CC BY 4.0.

shown in the first row of figure 9(TCV), and in the following two rows (AUG), respectively. The profiles of the PT scenario predicted by ASTRA-TGLF were flattened for $\rho_{tor} < 0.3$, approximately inside the $q = 1$ magnetic surface, to mimic the presence of the sawteeth, and better match the experiment. For TCV, ASTRA-TGLF with boundary conditions at $\rho_{tor} = 0.95$ reproduces the electron n, T profiles (figure 9(*a*)/(*c*)) reasonably well both for PT and NT shots, while it underestimates the ion temperature (figure 9(*b*)). ASTRA-TGLF is able to partially reproduce the beneficial effect coming from NT shape, but when looking at the logarithmic gradients, this effect is confined to the very edge $\rho_{tor} > 0.98$ [19], much outside the region $\rho_{tor} > 0.9$ where the beneficial effect of NT is seen in the experimental data. Therefore, it seems mainly related to the improved boundary condition.

On the contrary, for AUG, ASTRA-TGLF with boundary conditions at $\rho_{tor} = 0.85$ for the H-modes and $\rho_{tor} = 0.95$ for the L-mode is able to reproduce very well the experimental data, as is shown in 9(*d*)–(*f*) and (*g*)–(*i*), corresponding to the ECRH-only cases with higher and lower injected power, respectively. The ASTRA-TGLF runs also give us important information about the predicted T_i profiles, that are not measured except for the lower power #40473 NT pulse. The fact that the prediction agrees with the experiment for that case is encouraging, and we can thus use the T_i predictions to have a prediction of the total pressure or the ion pressure, as we anticipated earlier in the text. However, as shown in the following, this does not mean that TGLF can explain the better performance of some of the NT pulses in terms of reversed triangularity.

Indeed, for all DTT, TCV and AUG cases, a numerical experiment was performed, by flipping the LCFS shape of NT and PT around the magnetic axis. For DTT, a beneficial effect of NT was only found when flipping the LCFS of the PT up-down symmetric and higher-δ shape, mostly improving the central T_e for NT. For TCV, an even larger beneficial effect, compared with DTT, is only found when flipping the PT shape, only impacting n_e and T_i. For AUG, a beneficial effect of NT was found when flipping the PT shape, and a smaller but non-negligible one when flipping the NT shape. The larger

beneficial effect that is found when flipping the PT shape is explained in [19, 20] as due to the fact that not only the absolute value of the triangularity of the NT cases is smaller than the PT ones, but in addition, the DTT NT shape is highly up-down asymmetric. Therefore, the up-down symmetric Miller equilibrium that TGLF uses as an approximation for the real one, misses more than half of the upper NT, since it averages it with the lower triangularity, which is slightly positive. This way, the NT shape is poorly modeled by TGLF and the effect of reversing it is in great part lost. On the contrary, TGLF correctly represents the PT up-down symmetric shape and, therefore, it recovers the beneficial effect of flipping it, reversing the triangularity.

Summing up, only part of the beneficial effect of NT that is seen in the experiments is explained by ASTRA-TGLF as coming from the change of δ alone, and the rest could come from a better performance of NT in the edge-SOL, as discussed before, or by the fact that TGLF is badly approximating the up-down asymmetric DTT NT shape with an up-down symmetric Miller equilibrium.

2.4. Effect of NT on energy confinement: 0D parameters

To estimate the change in plasma confinement properties when changing the triangularity, it is useful to introduce 0D parameters such as the energy confinement time τ_E =(plasma stored energy/rate of energy loss) and the normalized beta $\beta_N = \beta(aB_t/I_p)$, where β =(total kinetic pressure/magnetic pressure) and a is the minor radius. The results are collected in the last two bars of figure 10 plots, for the DTT (a), TCV (b) and AUG (c)/(d). One notes that only when comparing the TCV PT/NT L-modes one has larger τ_E and β_N for NT. For all the other cases, the NT values stay below the PT ones. When comparing PT H-modes with NT L-modes, this is partially due to the fact that these 0D parameters are proportional to the integral of the pressure over the whole plasma volume, and the presence of the pressure pedestal for the H-modes heavily impacts the PT/NT comparison. Even for the AUG high ECRH power PT/NT H-mode/H-mode comparison, the NT H-mode presents a much smaller pedestal compared with the PT H-mode.

However, since the fusion power density is proportional to p_i^2 ([44], equations 1.4.1, 1.5.4), and most of the neutron fusion production is confined in the inner core, a better fusion performance is obtained when larger pressures/temperatures are reached in the plasma central region. Therefore, the average values of p_i in the plasma central region are more meaningful than τ_E and β_N when comparing discharges with very different edge conditions, since τ_E and β_N, as discussed before, give large weight to the plasma edge, which does not produce fusion neutrons. With that in mind, we shall consider here the average of p_i^2 over the central plasma region, defined by

$$\langle p_i^2 \rangle = \frac{1}{V}\int_0^{0.4} p_i^2 \frac{dV}{d\rho_{tor}} d\rho_{tor} \quad (4)$$

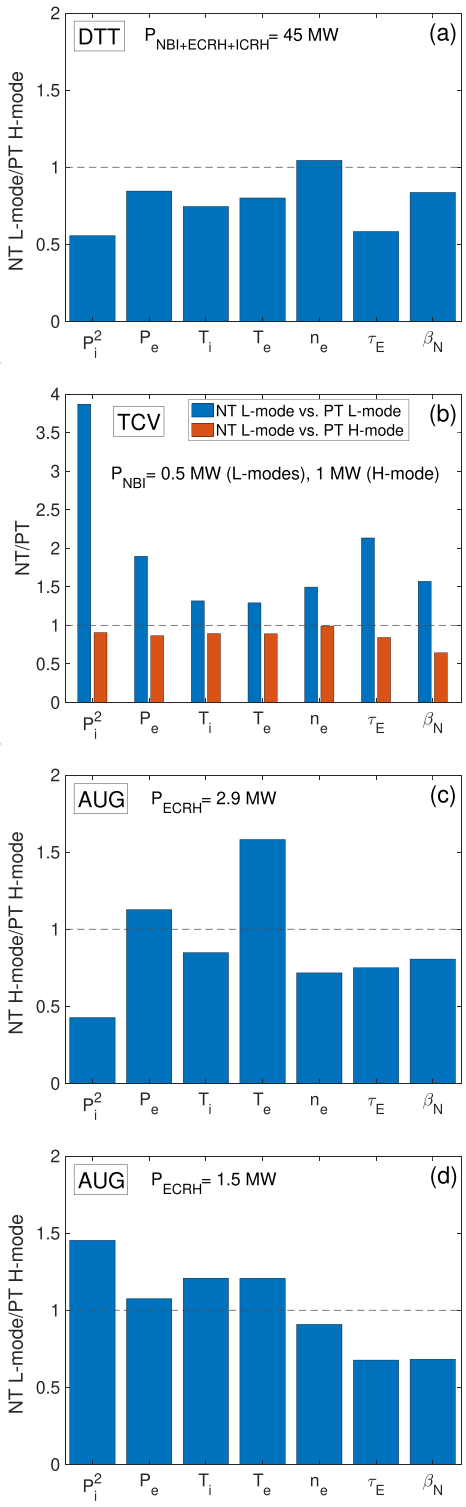

Figure 10. Zero-dimensional parameters: ratio of NT geometry and PT geometry values. The dashed black line marks a ratio of 1, for which the two configurations would have the same performance. (a) DTT PT/NT scenarios; (b) TCV NBI-only discharges; (c) AUG ECRH-only higher power discharges; (g)–(i) AUG ECRH-only lower power discharges. (b) Reproduced from [19]. © The Author(s). Published by IOP Publishing Ltd. CC BY 4.0.

with V the volume enclosed by the $\rho_{tor} = 0.4$ magnetic surface, as a measure of the plasma performance when comparing PT with NT plasmas. The region $0.2 < \rho_{tor} < 0.4$ mainly

contributes to the volume integrals, since the volume enclosed within $\rho_{\rm tor} = 0.2$ is relatively small. These values are shown by the first bars of figure 10 graphs. More information on the main kinetic profiles contributing $p_{\rm i}$ and $p_{\rm tot}$ is also given in the intermediate bars, i.e. the values of $\langle p_{\rm e}\rangle$, $\langle T_{\rm e}\rangle$, $\langle T_{\rm i}\rangle$ and $\langle n_{\rm e}\rangle$, with $\langle\cdots\rangle$ defined as in equation (4). The $\langle\cdots\rangle$ brackets were omitted in figure 10 for brevity. One observes that while for DTT $\langle p_{\rm i}^2\rangle$ is still much lower for the NT case compared with the PT one, for TCV NT L-mode it almost reaches the double NBI power PT H-mode, exceeding by almost four times the corresponding PT L-mode with the same power. When one also considers the TCV cases with ECRH-only and mixed NBI/ECRH heating mix, which are here not shown for brevity, the NT L-modes always have larger $\tau_{\rm E}$, $\beta_{\rm N}$ and $p_{\rm i}^2$ than the corresponding PT L-modes, positioning themselves between the PT L-modes and the higher power PT H-modes [19]. For the AUG ECRH-only case with higher power (figure 10(*c*)), as anticipated earlier, the lower density of the NT case reduces the electron-ion heat exchange compared with the PT case, leading also to a lower $T_{\rm i}$ and a corresponding much lower $p_{\rm i}^2$. On the contrary, for the lower power case (figure 10(*d*)), the slightly lower density for the NT L-mode case is more than compensated by the larger $T_{\rm i}$, leading to a larger $p_{\rm i}^2$.

3. Gyrokinetic simulations

Linear and nonlinear flux-tube gyrokinetic simulations were performed with the GENE code at fixed radii for DTT and TCV, while some preliminary runs are ongoing for AUG, to validate the ASTRA-TGLF runs and/or interpret the experiments. Let us first consider the linear results. The GENE runs were performed including kinetic electrons, electromagnetic effects, collisions (Landau operator) and impurities (DTT: Ne and W, TCV: C). Positive/negative values of the real frequency correspond to modes rotating in the ion/electron diamagnetic direction, respectively.

3.1. Linear simulations

For DTT, linear scans in the poloidal wavenumber were carried out at two radii, $\rho_{\rm tor} = 0.7, 0.85$, where $|\delta|$ was supposed to be sufficiently large to impact the transport. For each radius, two additional shapes were considered, in addition to the PT and NT ones, obtained by rigidly flipping the LCFS with respect to the cylinder identified by the magnetic axis, and then recomputing the equilibrium inside it with CHEASE. The micro-instability regime is found to be ITG-dominant at both radii, and a strong stabilizing effect, that halves the growth rates, is found when flipping the triangularity in H-mode with fixed PT profiles, while a negligible effect of flipping δ is found in the L-mode. The linear growth rates and frequencies at $\rho_{\rm tor} = 0.85$, where the triangularity is larger and has a larger impact, are shown in the first column of figure 11.

For TCV, since an improvement of the logarithmic gradients of $T_{\rm e}$, $T_{\rm i}$ and $n_{\rm e}$ for the NT L-mode compared with the PT L-mode was observed for $\rho_{\rm tor} > 0.9$, as mentioned above, a similar exercise was performed at $\rho_{\rm tor} = 0.95$ [19]. For TCV, the PT and NT shapes were switched, instead of flipping them with respect to the magnetic axis. In addition, since a large stabilizing effect of NT is found at $\rho_{\rm tor} = 0.95$, the linear scans were repeated at the smaller radius $\rho_{\rm tor} = 0.8$, close to the TCV radius of analysis (new results, unpublished). The TCV linear eigenvalues at $\rho_{\rm tor} = 0.8$ and $\rho_{\rm tor} = 0.95$ are shown in the second and third columns of figure 11, respectively. At both radii, for the considered NBI-only case, a continuous TEM-ITG branch is found in all the cases except for the NT L-mode at $\rho_{\rm tor} = 0.8$, which presents negative frequency at every wavenumber. The frequencies are more negative for the NT cases. We also report that a TEM-dominant micro-instability regime is found at $\rho_{\rm tor} = 0.85$ for the mixed ECRH/NBI and pure ECRH cases [19]. We also report that preliminary GENE linear scans neglecting impurities and TGLF SAT2 runs show that for the AUG ECRH-only pulses the micro-instability regime is ITG-dominant, due to a large electron-ion equipartition that increases $q_{\rm i}/q_{\rm e}$. Looking at the growth rates, a large beneficial effect is found at the larger radius, even though it is still strong at $\rho_{\rm tor} = 0.8$, when switching the shape starting from the PT case.

Finally, to better compare with the TCV analysis, a test was performed for DTT, by switching the PT/NT shapes instead of flipping them, and it is shown by crosses in (*a*)/(*d*). These are new results, not present in [18]. One sees that flipping or switching the shape gives similar results at the smaller-k values that contribute to the nonlinear fluxes when starting from the NT case, while switching the PT shape with the NT 'teardrop' one strongly reduces the stabilizing effect of NT that is seen when flipping the PT up-down symmetric shape. This means that for the DTT PT H-mode parameters an up-down symmetric negative shape with slightly larger $|\delta|$ would be much more beneficial than the one considered for the DTT NT scenario. However, this consideration is of little practical utility, since probably, when flipping the shape, the PT pedestal would be much reduced and the parameters at $\rho_{\rm tor} = 0.85$ would change.

3.2. Nonlinear simulations

Nonlinear GENE simulations were performed for DTT and TCV, to estimate the effect of the NT on the heat transport. First of all, the turbulence regime was better characterized by looking at the electron/ions heat flux ratio $q_{\rm e}/q_{\rm i}$ from GENE nonlinear simulations, for the DTT and TCV cases of figure 11, with the following results: $q_{\rm e}/q_{\rm i} = 0.54/0.46$ (DTT PT H-mode/NT L-mode at $\rho_{\rm tor} = 0.85$), 0.77/1.62 (TCV PT L-mode/NT L-mode at $\rho_{\rm tor} = 0.8$), 1.05/1.85 (TCV PT L-mode/NT L-mode at $\rho_{\rm tor} = 0.95$). Therefore, the DTT cases are ITG-dominant ($q_{\rm i} > q_{\rm e}$), the TCV NT L-modes are TEM-dominant ($q_{\rm e} > q_{\rm i}$), while the TCV PT L-modes with continuous linear TEM-ITG branch with frequencies close to zero present a more balanced ITG-TEM behavior $q_{\rm e} \sim q_{\rm i}$.

Figure 12(*a*) and (*b*) show the details of the total heat fluxes, split in electron and ion contributions, corresponding to the linear simulations in the first and last column of figure 11.

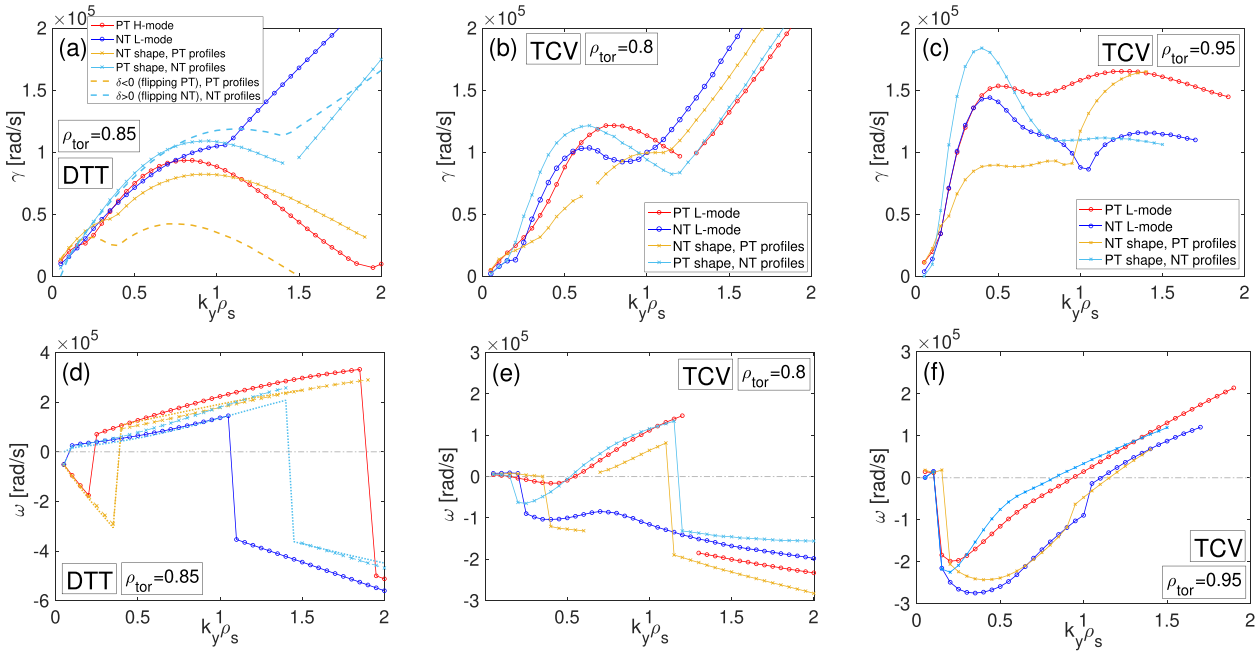

Figure 11. GENE linear k_y spectra of the growth rate γ and frequency ω of the most unstable mode, for DTT at $\rho_{\rm tor} = 0.85$ (first column), TCV NBI-only at $\rho_{\rm tor} = 0.8$ (second column), and TCV NBI-only at $\rho_{\rm tor} = 0.95$ (third column). (*a*)/(*d*) Reproduced from [18]. © 2024 The Author(s). Published by IOP Publishing Ltd on behalf of the IAEA. All rights reserved CC BY 4.0. (the data with crosses are new). (*c*)/(*f*) Reproduced from [19]. © The Author(s). Published by IOP Publishing Ltd. CC BY 4.0.

Only the 'flipped' PT/NT counterparts are shown for DTT, corresponding to the simulations of [18]. The total heat flux is reduced by 67% in H-mode when flipping δ starting from PT, even more than the linear stabilizing effect on the growth rates, while the effect is negligible when flipping the NT L-mode, consistently with the linear analysis (figure 11(*a*)).

The ion temperature stiffness, i.e. the degree to which the radial $T_{\rm i}$ profile responds to changes in the applied heat fluxes, was studied for DTT scenarios at $\rho_{\rm tor} = 0.85$, given that the micro-instability regime was found to be ITG-dominant with the linear analysis, and the main ITG drive is $a/L_{T{\rm i}}$. The results are summarized in figure 12(*c*), where GENE scans of the ion heat flux $q_{\rm i}$ versus $a/L_{T{\rm i}}$ are shown for the four considered shapes. An effect of flipping the shape alone is only found for the H-modes, where a $+36\%$ increase of $a/L_{T{\rm i}}$ is obtained when flipping the PT H-mode. The agreement of GENE with ASTRA-TGLF (stars in the figure) is good at the ASTRA-TGLF flux level, therefore, the predictive transport analysis is validated by GENE at the radius of analysis. Recalling that for the AUG PT/NT H-modes a stabilizing effect of NT is observed in the $0.7 < \rho_{\rm tor} < 0.9$ region, one could consider the hypothesis that for H-mode parameters the beneficial effect of NT could penetrate to inner radii compared with L-mode parameters. Simulations were performed to understand which are the key parameters that explain the larger effect of NT in DTT when considering the PT H-mode kinetic profiles, compared with the L-mode ones. The collisionality, which was at first identified as the only parameter that was able to explain a beneficial effect of NT, was ruled out by a new GENE collisionality scan. However, this scan did not include impurities, for lack of computational resources. Therefore, there is still room for further investigation in this direction.

Turning to TCV, the total heat flux is reduced by 59% when switching the shape starting from the PT L-mode, keeping fixed the kinetic profiles, while it is increased by $+53\%$ when switching the shape starting from the NT L-mode and keeping fixed the kinetic profiles (figure 12(*b*)). This means that for TCV at $\rho_{\rm tor} = 0.95$, differently from DTT at the smaller radius $\rho_{\rm tor} = 0.85$, the beneficial effect of NT is present for the L-mode, and it can be seen both keeping fixed the PT or the NT L-mode profiles. This is also consistent with the linear results. The temperature stiffness is then investigated for TCV, with results shown in figure 12(*d*). The $T_{\rm e}$ stiffness is investigated instead of the $T_{\rm i}$ one since, for TCV, the turbulence is found to be mixed ITG/TEM, with NT L-mode being more TEM dominated, and the TEM main drive is $a/L_{T{\rm e}}$. In figure 12(*d*) the stars indicate the experimental values. In contrast with what was observed in DTT NT L-mode at $\rho_{\rm tor} = 0.85$, TCV at $\rho_{\rm tor} = 0.95$ shows a direct effect of the triangularity on the electron heat transport. Indeed, switching the triangularity from positive to negative shape leads to a $+135\%$ increase of $a/L_{T{\rm e}}$ when keeping fixed the NT L-mode profiles, while a $+85\%$ effect is predicted with PT L-mode profiles. This direct effect of NT, predicted by gyrokinetics, is much larger than the $\sim +10\%$ experimental increase of $a/L_{T{\rm e}}$ that is seen when going from PT to NT L-mode (compare the two stars). This means that

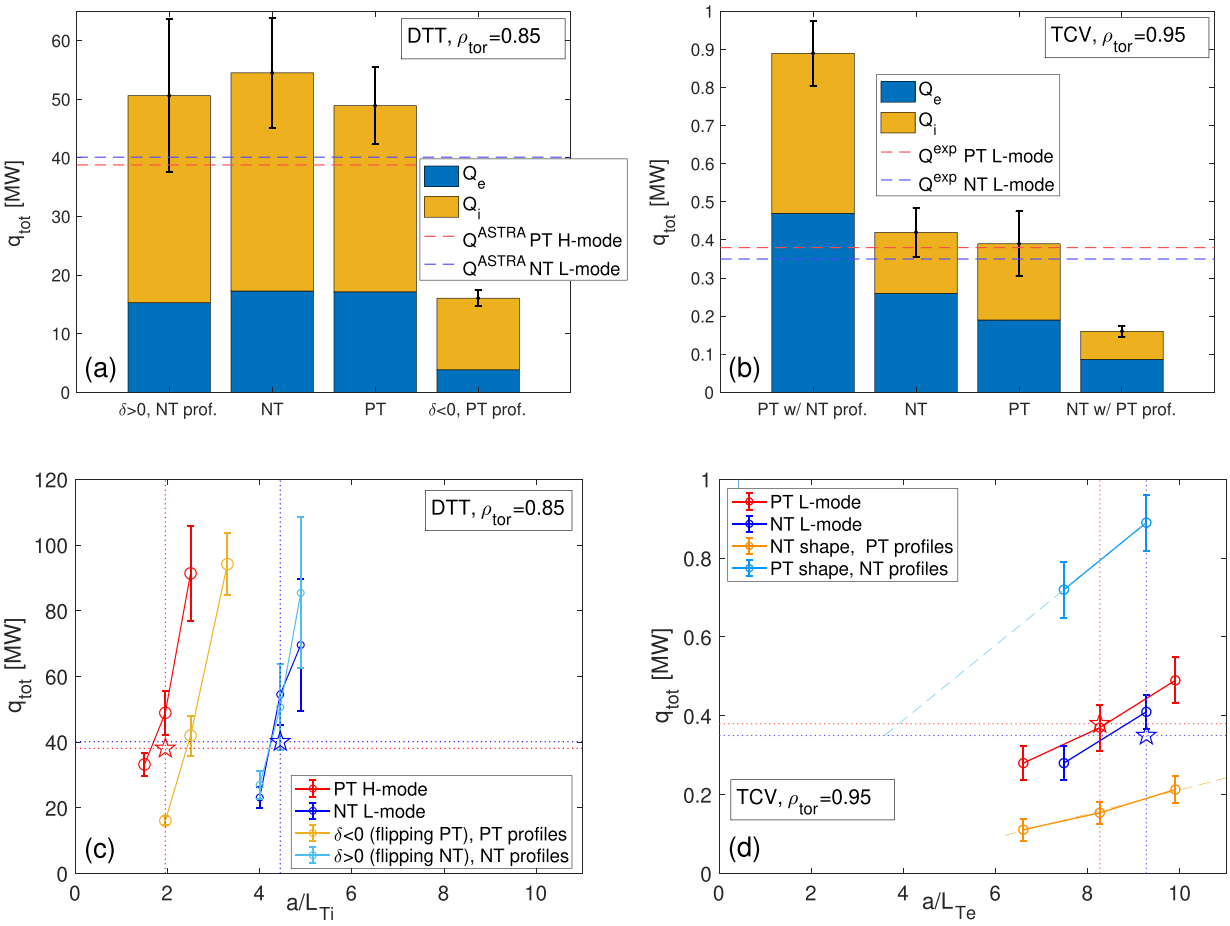

Figure 12. Nonlinear GENE simulations. (*a*) and (*b*) total heat fluxes, splitted in electron (blue) and ion (yellow) contributions, for DTT at $\rho_{tor} = 0.85$ and TCV at $\rho_{tor} = 0.95$, respectively. The red and blue dashed lines for DTT indicate the predicted fluxes by ASTRA-TGLF, while for TCV they show the experimental fluxes. (*c*) and (*d*) T_i stiffness plot for DTT and T_e stiffness plot for TCV, varying only the temperature logarithmic gradients, starting from the reference parameters of (*a*) and (*b*), respectively. The total heat flux is reported as a function of the logarithmic gradients a/L_{Ti} and a/L_{Te} for DTT and TCV, respectively. The dashed lines are a prolongation of the solid lines to find the intercept with the *x*-axis. The dotted blue and red horizontal lines for TCV are the experimental heat fluxes, while the vertical ones are the experimental gradients of PT (red) and NT (blue). The stars represent the point where the vertical and horizontal lines meet. For DTT, instead of the experimental values, the predicted ones by ASTRA-TGLF are shown. (*b*)/(*d*) Reproduced from [19]. while (*c*) Reproduced from [18].

there is a large beneficial effect of NT, but the different kinetic profiles for the two TCV L-modes with PT/NT partially compensate for this effect.

As a summary, GENE linear and nonlinear simulations seem to explain the beneficial effect of NT that is experimentally observed at $\rho_{tor} = 0.95$ for TCV NBI-only L-modes, as a direct effect of NT, partially reduced by the different kinetic profiles that are obtained with the two configurations. The linear TCV simulations at $\rho_{tor} = 0.8$ find a much smaller beneficial effect of NT compared with those at $\rho_{tor} = 0.95$. Similarly, DTT could show a benefit of reversing δ at $\rho_{tor} > 0.85$. This will require further analysis. The fact that in TCV turbulence is TEM-dominated (at least when considering the NT L-modes), while in DTT it is mostly ITG-dominated, could be the reason for improved performance of NT in TCV. However, this is in contrast with the picture emerging from the work of the TSVV2 group, where similar effects are found in reversing δ both in ITG and TEM regimes [11]. Moreover, if we look, for example, to the linear simulations of TCV at $\rho_{tor} = 0.8$, a smaller beneficial effect of NT is found when keeping NT L-mode profiles, that lead to a TEM-dominant regime, compared with the effect obtained with PT profiles, corresponding to a mixed ITG/TEM regime. The rather large increase of T_e peaking of TCV NT L-mode compared with the PT L-mode at $\rho_{tor} > 0.9$ could be principally due to the effect of NT combined with the lower stiffness in the edge region [45], that allows temperature to peak. The much smaller T stiffness (i.e. the smaller slope of q_{tot} vs a/L_T) of TCV cases at $\rho_{tor} = 0.95$ compared with DTT cases at $\rho_{tor} = 0.85$ can be clearly seen by comparing figures 12(*c*) and (*d*). Therefore, there is still room for the DTT NT scenario to have a beneficial effect of NT coming from the outer edge. As a caveat, a similar analysis of the temperature stiffness by means of a/L_T scans of nonlinear gyrokinetic simulations should also be performed for DTT at $\rho_{tor} = 0.95$

and for TCV at $\rho_{\rm tor} = 0.85$, to exclude the possibility that the dependence of the temperature stiffness on the radial position could be different for the two cases. This has not yet been done for lack of computational resources, and is left as future work.

4. Conclusions

A NT option for the DTT full-power scenario is under design, to achieve high plasma performance without the ELMs, which are predicted to be unstable in the standard H-mode scenario with PT. The heat transport properties of the DTT NT scenario are here investigated by means of predictive ASTRA-TGLF simulations and gyrokinetic GENE runs. In addition, recent dedicated experiments with similar shapes to the DTT PT/NT scenarios were performed at TCV/AUG and interpreted with ASTRA-TGLF and GENE simulations. All these results are collected and compared in this work, in order to get insight into the viability and the performance of the DTT NT scenario. The main outcomes of the analysis and the possible future work are summarized in the following.

- ASTRA-TGLF SAT2 predictive transport simulations with boundary conditions at $\rho_{tor} = 0.94$ predict that in the NT L-mode DTT full-power scenario the $|\delta|$ value is too small to allow density and temperature profiles to overcome the loss of the PT H-mode pedestal and reach similar central values: this picture is confirmed by GENE simulations up to $\rho_{\rm tor} = 0.85$. A new NT scenario with larger negative upper triangularity and reduced volume to satisfy DTT engineering constraints is thus under development.
- TCV experiments with DTT-like shapes: large beneficial effect of NT for different power mixes (ECRH, ECRH/NBI and NBI), with NT L-modes that outperform corresponding PT L-modes and reach central pressures similar to PT H-modes with twice the power. This could seem in contrast with the DTT numerical analysis. However, the effect of changing the sign of triangularity on TCV experiments is limited to the edge-SOL region $\rho_{\rm tor} > 0.8$, with some cases that show this effect only for $\rho_{\rm tor} > 0.9$. Therefore, this effect could simply have been missed in DTT simulations. Some additional stabilizing effect of NT could come from $\rho_{\rm tor} > 0.94$ for DTT, outside the boundary of the ASTRA-TGLF simulation domain, and/or TGLF could miss part of the effect of the NT since it uses an up-down symmetric Miller equilibrium, poorly representing the up-down asymmetric 'teardrop' shape of the DTT NT scenario. New interfaces to TGLF are being developed in present transport codes, capable of modeling realistic up-down asymmetric shapes. However, the NT option should still not access H-mode-like pedestals due to the inhibited access to the second stability region of high-n ballooning modes for sufficiently negative δ and thus not lead to ELMs.
- AUG experiments tend to go into H-mode even with NT shapes in favorable configuration. The AUG plasmas with NT shapes always present much lower or absent pressure pedestals, corresponding to much weaker or absent ELM activity, compared with PT plasmas with the same input power. Overall, for AUG, a smaller beneficial effect of NT is found, compared with TCV. Only for a pair of ECRH heated PT/NT pulses with DTT-like shapes with relatively low power, the NT plasma outperforms the corresponding PT one in terms of the average ion pressure in the inner core, which is related to neutron production and, therefore, to fusion performance. The reason for this difference with TCV has still to be understood. One possible explanation is the different wall materials (C for TCV, W for AUG), which should lead to further studies about the effect of those impurities on the edge transport. Another possibility is that finite size effects could play a role on TCV, due to its relatively small size. For these reasons, global GENE nonlinear simulations of the TCV NBI only PT/NT pulses are ongoing, and the results will be compared with the radially local ones at $\rho_{\rm tor} = 0.8, 0.95$. However, this second possible reason seems unlikely, since the TCV PT-NT L-modes at $\rho_{\rm tor} = 0.95$ display rather small $\rho^* = \rho_{\rm s}/a \sim 1/357 - 1/278$ values, and the flux-tube GENE runs seem already to overpredict the beneficial effect of NT.
- For the considered TCV and AUG discharges with DTT-like shapes, it follows by an inspection of the logarithmic gradients of the main kinetic profiles inside the separatrix that a beneficial effect of NT comes from reduced transport in the edge region $\rho_{\rm tor} > 0.8$ when comparing PT/NT L-modes while, when comparing PT/NT H-modes, the beneficial effect starts more inside ($\rho_{\rm tor} < 0.9$).
- GENE linear simulations: a large beneficial effect of the triangularity, which strongly reduces the linear growth rates, is only found for TCV at $\rho_{\rm tor} = 0.95$ and for DTT at $\rho_{\rm tor} = 0.85$ when the PT shape is flipped around the magnetic axis. For the other cases, the effect is milder, and absent when flipping the shape of the DTT NT scenario, or switching it with the PT one. This confirms the experimentally measured beneficial effect of NT for TCV at $\rho_{\rm tor} = 0.95$, and indicates that at smaller radii the effect could be smaller, as it is found for DTT. The micro-instability regime is found to be ITG-dominant for DTT, while it is mixed TEM/ITG for TCV. Preliminary linear GENE runs neglecting impurities and TGLF simulations indicate that the AUG regime should be ITG-dominant in the plasma edge for the ECRH-only cases, due to a large electron-ion heat exchange that transfers energy to the ions.
- GENE nonlinear simulations: based on the analysis of the ratio of electron and ion heat fluxes ($q_{\rm e}/q_{\rm i} < 1$ for ITG-dominant turbulence, while $q_{\rm e}/q_{\rm i} > 1$ when TEM-dominant), DTT is confirmed to be ITG-dominant at the radii of analysis, TCV PT cases are found to be mixed TEM/ITG and the TCV NT cases to be TEM-dominant. However, the stabilizing effect of NT seems independent of the most unstable micro-instability. The ion temperature stiffness is then investigated for DTT, which is ITG-dominant, while the electron temperature stiffness for TCV, that is more TEM-dominant overall. The strong beneficial effect that was found with linear simulations for TCV at $\rho_{\rm tor} = 0.95$ is confirmed, even overpredicting the increase in $a/L_{T\rm e}$ when going from PT to NT that is found in the experiment. This means that the experimental beneficial effect of

NT is explained by the simulations, as a very strong direct effect of changing the shape, partially compensated by the change of other parameters between the PT/NT pulses. Consistently with the linear analysis, a beneficial effect of NT is only found for DTT at $\rho_{tor} = 0.85$ when flipping the shape starting from the PT H-mode scenario. Since also for AUG PT/NT H-modes a stabilizing effect of NT is observed in the $0.7 < \rho_{tor} < 0.9$ region, it is possible that for H-mode parameters, the beneficial effect of NT could penetrate to inner radii compared with L-mode parameters.

Summing up, the DTT simulations and the TCV/AUG experiments/simulations with DTT-like shapes indicate that a possible beneficial effect of operating the DTT full-power scenario with NT could come from the plasma edge-SOL, allowing the NT scenario to achieve central pressure values comparable to the reference PT H-mode, staying in L-mode or presenting a reduced pedestal, thus showing a much weaker or even absent ELM activity. Even without this additional beneficial effect coming from the edge-SOL, the NT option is predicted to provide high performance plasmas with reduced or absent ELMs, resulting in a viable alternative for the DTT full power scenario. However, since the extrapolability of the performance of experimental NT scenarios to different tokamaks is not granted at present, turbulence simulations of the edge-SOL of TCV/AUG and DTT, consistently modeling the region across the separatrix, are needed to confirm this (ongoing work). In addition, it would be useful to perform further flux-tube gyrokinetic simulations for the various machines at the same radii, to improve the understanding on how to extrapolate results from one machine to another. This would also allow to better compare important properties of the kinetic profiles among different machines, such as the radial dependence of the temperature stiffness, which could strongly influence the beneficial effect of NT at larger radii. Then, the different size of the improvement of plasma performance in NT compared to PT for TCV and AUG experiments, with a larger beneficial effect which is found for TCV, is still to be understood, and the impact of the main differences of the two tokamaks has still to be quantified. In particular, the impact of the different wall materials has to be studied. Finally, in order to attempt improving the penetration depth of the beneficial effect of NT inside the separatrix down to the core, a new shape for the DTT NT scenario is under design, with double upper NT and reduced volume to meet the engineering constraint of the DTT tokamak. TCV pulses with this new shape are also planned to experimentally test its performance.

Acknowledgments

This work was carried out within the framework of the EUROfusion Consortium, partially funded by the European Union via the Euratom Research and Training Programme (Grant Agreement No 101052200 - EUROfusion). The Swiss contribution to this work was funded by the Swiss State Secretariat for Education, Research and Innovation (SERI). Views and opinions expressed are however those of the author(s) only and do not necessarily reflect those of the European Union, the European Commission or SERI. Neither the European Union nor the European Commission nor SERI can be held responsible for them. This work was supported in part by the Swiss National Science Foundation. We acknowledge the CINECA award under the ISCRA initiative and the EUROfusion WP-AC, for the availability of high performance computing resources and support. This work was performed within the TSVV-02 EUROfusion task. Some figures, as indicated in the captions, are adapted, with permission, from [18, 19] and [20].

ORCID iDs

A. Mariani https://orcid.org/0000-0003-0476-3825
L. Aucone https://orcid.org/0000-0003-3949-678X
A. Balestri https://orcid.org/0009-0009-8309-7736
P. Mantica https://orcid.org/0000-0001-5939-5244
G. Merlo https://orcid.org/0000-0003-4877-1456
L. Balbinot https://orcid.org/0000-0002-7467-533X
J. Ball https://orcid.org/0000-0002-4462-6350
T. Bolzonella https://orcid.org/0000-0003-1128-964X
I. Casiraghi https://orcid.org/0000-0002-1719-6682
S. Coda https://orcid.org/0000-0002-8010-4971
L. Frassinetti https://orcid.org/0000-0002-9546-4494
V. Fusco https://orcid.org/0000-0003-1179-4363
T. Happel https://orcid.org/0000-0003-4364-9363
J. Hobirk https://orcid.org/0000-0001-6605-0068
R.M. McDermott https://orcid.org/0000-0002-8958-8714
T. Pütterich https://orcid.org/0000-0002-8487-4973
O. Sauter https://orcid.org/0000-0002-0099-6675
F. Sciortino https://orcid.org/0000-0002-5159-1889
M. Vallar https://orcid.org/0000-0002-1792-6702
N. Vianello https://orcid.org/0000-0003-4401-5346
G. Vlad https://orcid.org/000-0003-1482-5436
C.F.B. Zimmermann https://orcid.org/0000-0003-3143-1471

References

[1] Camenen Y., Pochelon A., Bottino A., Coda S., Ryter F., Sauter O., Behn R., Goodman T.P., Henderson M.A. and Karpushov A. 2005 *Plasma Phys. Control. Fusion* **47** 1971
[2] Camenen Y., Pochelon A., Behn R., Bottino A., Bortolon A., Coda S., Karpushov A., Sauter O. and Zhuang G. (the TCV team) 2007 *Nucl. Fusion* **47** 510
[3] Coda S., Merle A., Sauter O., Porte L., Bagnato F., Boedo J., Bolzonella T., Février O., Labit B. and Marinoni A. 2022 *Plasma Phys. Control. Fusion* **64** 014004
[4] Austin M.E., Marinoni A., Walker M.L., Brookman M.W., deGrassie J.S., Hyatt A.W., McKee G.R., Petty C.C., Rhodes T.L. and Smith S.P. 2019 *Phys. Rev. Lett.* **122** 115001
[5] Marinoni A., Austin M.E., Hyatt A.W., Walker M.L., Candy J., Chrystal C., Lasnier C.J., McKee G.R., Odstrčil T. and Petty C.C. 2019 *Phys. Plasmas* **26** 042515
[6] Marinoni A., Austin M.E., Hyatt A.W., Saarelma S., Scotti F., Yan Z., Chrystal C., Coda S., Glass F. and Hanson J.M. 2021 *Nucl. Fusion* **61** 116010

[7] Happel T., Pütterich T., Told D., Dunne M., Fischer R., Hobirk J., McDermott R.M. and Plank U. (the ASDEX Upgrade Team) 2023 *Nucl. Fusion* **63** 016002
[8] Marinoni A., Sauter O. and Coda S. 2021 *Rev. Mod Plasma Phys.* **5** 6
[9] Loarte A., Huijsmans G., Futatani S., Baylor L., Evans T., Orlov D.M., Schmitz O., Becoulet M., Cahyna P. and Gribov Y. 2014 *Nucl. Fusion* **54** 033007
[10] Eich T., Sieglin B., Thornton A.J., Faitsch M., Kirk A., Herrmann A. and Suttrop W. (JET contributors, MST contributors, ASDEX Upgrade and MAST teams) 2017 *Nucl. Mater. Energy* **12** 84–90
[11] Ball J. (behalf of the TSVV 2 team) Insights into a negative triangularity reactor from EUROfusion's TSVV 2 *7th Asia-Pacific Conf. on Plasma Physics* (*12–17 November 2023 at Port Messe Nagoya, Japan)* (available at: www.aappsdpp.org/DPP2023/)
[12] Medvedev S., Kikuchi M., Villard L., Takizuka T., Diamond P., Zushi H., Nagasaki K., Duan X., Wu Y. and Ivanov A. A. 2015 *Nucl. Fusion* **55** 063013
[13] Kikuchi M. *et al* 2019 *Nucl. Fusion* **59** 056017
[14] Casiraghi I., Mantica P., Koechl F., Ambrosino R., Baiocchi B., Castaldo A., Citrin J., Dicorato M., Frassinetti L. and Mariani A. 2021 *Nucl. Fusion* **61** 116068
[15] Ambrosino R. *et al* 2021 *Fusion Eng. Des.* **167** 112330
[16] Siccinio M. *et al* 2022 *Fusion Eng. Des.* **176** 113047
[17] Mariani A., Balestri A., Casiraghi I., Mantica P., Ambrosino R., Castaldo A., Balbinot L., Cipelli S., Frassinetti L. and Fusco V. 2022 *Poster at 48th European Physical Society (EPS) Conf. on Plasma Physics (Online, 27 June–1 July 2022)* (available at: www.eps.org/events/eventdetails.aspx?id=1635374)
[18] Mariani A., Balestri A., Mantica P., Merlo G., Ambrosino R., Balbinot L., Brioschi D., Casiraghi I., Castaldo A. and Frassinetti L. 2024 *Nucl. Fusion* **64** 046018
[19] Balestri A., Mantica P., Mariani A., Bagnato F., Bolzonella T., Ball J., Coda S., Dunne M., Faitsch M. and Innocente P. 2024 *Plasma Phys. Control. Fusion* **66** 065031
[20] Aucone L., Mantica P., Happel T., Hobirk J., Pütterich T., Vanovac B., Zimmermann C.F.B., Bernert M., Bolzonella T. and Cavedon M. 2024 *Plasma Phys. Control. Fusion* **66** 075013
[21] Pereverzev G.V. and Yushmanov P.N. 2002 ASTRA automated system for transport analysis in a tokamak *IPP Report 5/98* Max-Planck-Institut für Plasmaphysik
[22] Fable E., Angioni C., Casson F.J., Told D., Ivanov A.A., Jenko F., McDermott R.M., Medvedev S., Pereverzev G.V. and Ryter F. 2013 *Plasma Phys. Control. Fusion* **55** 124028
[23] Staebler G.M., Candy J., Howard N.T. and Holland C. 2016 *Phys. Plasmas* **23** 062518
[24] Jenko F., Dorland W., Kotschenreuther M. and Rogers B.N. 2000 *Phys. Plasmas* **7** 1904
[25] Görler T., Lapillonne X., Brunner S., Dannert T., Jenko F., Merz F. and Told D. 2011 *J. Comput. Phys.* **230** 7053
[26] Casiraghi I., Mantica P., Ambrosino R., Aucone L., Baiocchi B., Balbinot L., Barberis T., Castaldo A., Cavedon M. and Frassinetti L. 2023 *Plasma Phys. Control. Fusion* **65** 035017
[27] Albanese R., Ambrosino R. and Mattei M. 2015 *Fusion Eng. Des.* **96–97** 664–7
[28] Ivanov A. A. 2005 *32nd EPS Conf. on Plasma Physics-Terragona 29C* (ECA) p-5.063 (available at: https://info.fusion.ciemat.es/eps05/)
[29] Moret J.-M., Duval B.P., Le H.B., Coda S., Felici F. and Reimerdes H. 2015 *Fusion Eng. Des.* **91** 1
[30] Fischer R. *et al* 2013 *40th EPS Conf. on Plasma Physics-Espoo* (Finland) p -2.139 (available at: www.eps.org/events/EventDetails.aspx?id=287375)
[31] Merle A., Sauter O. and Medvedev S. 2017 *Plasma Phys. Control. Fusion* **59** 104001
[32] Saarelma S., Austin M.E., Knolker M., Marinoni A., Paz-Soldan C., Schmitz L. and Snyder P.B. 2021 *Plasma Phys. Control. Fusion* **63** 105006
[33] Nelson A.O., Paz-Soldan C. and Saarelma S. 2022 *Nucl. Fusion* **62** 096020
[34] Nelson A.O., Schmitz L., Paz-Soldan C. , Thome K.E., Cote T.B., Leuthold N., Scotti F., Austin M.E. , Hyatt A. and Osborne T. 2023 *Phys. Rev. Lett.* **131** 195101
[35] Sauter O. *et al* 2023 Negative triangularity tokamak operation in TCV *Oral at 29th IAEA Fusion Energy Conf.* (*London, United Kingdom, 16–21 October 2023*) (available at: www.iaea.org/events/fec2023)
[36] Sauter O. 2016 *Fusion Eng. Des.* **112** 633
[37] Vanovac B. *et al* 2023 *EPJ Web Conf.* **277** 03003
[38] Gil L., Silva C., Happel T., Birkenmeier G., Conway G.D., Guimarais L., Kallenbach A., Pütterich T., Santos J. and Schneider P.A. 2020 *Nucl. Fusion* **60** 054003
[39] Vanovac B. *et al* 2023 Pedestal properties of negative triangularity plasma in AUG *27th Joint EU-US Transport Task Force Meeting (Nancy, France, 11–15 September 2023)*
[40] Merlo G., Huang Z., Marini C., Brunner S., Coda S., Hatch D., Jarema D., Jenko F., Sauter O. and Villard L. 2021 *Plasma Phys. Control. Fusion* **63** 044001
[41] Ball J. and Brunner S. 2023 *Plasma Phys. Control. Fusion* **65** 014004
[42] Muscente P. *et al* 2023 *Poster Contribution to the 49th European Conf. on Plasma Physics* (EPS)
[43] Lim K., Giacomin M., Ricci P., Coelho A., Février O., Mancini D., Silvagni D. and Stenger L. 2023 *Plasma Phys. Control. Fusion* **65** 085006
[44] Wesson J. 2003 *Tokamaks* 3rd edn (Clarendon)
[45] Sauter O., Brunner S., Kim D., Merlo G., Behn R., Camenen Y., Coda S., Duval B.P., Federspiel L. and Goodman T.P. 2014 *Phys. Plasmas* **21** 055906